JCTC Journal of Chemical Theory and Computation

Tunneling Dynamics in a Double-Well Model of an H Transfer Reaction

Ashley E. Myers, Matt R. Teague, and Michael Messina*

Department of Chemistry and Biochemistry, University of North Carolina, Wilmington, North Carolina 28403

Received October 15, 2008

Abstract: We study the role that tunneling can play in the reaction dynamics of H atom transfer. The small mass of the H atom offers it another, nonclassical route, from reactants to products, tunneling through an activation barrier. In this work, we carefully define the portion of a reaction rate constant that is caused by tunneling in such reactions. We do this by decomposing an initial H atom wavepacket into above and below the barrier components. We show that for a very particular decomposition, the quantum dynamics of the system can be separated into two events: tunneling and above-the-barrier product production. We show for such decomposition it is possible to determine a rate constant because of tunneling alone. Finally, we demonstrate that from a single experimental observable, the overall decay of reactant concentration, one can extract structural and dynamical information about the H atom transfer reaction.

I. Introduction

Recently there has been great interest in the role tunneling plays in reaction dynamics, particularly enzyme catalyzed H transfer reactions.[1−10] As is well-known, the small mass of the H atom offers it another, nonclassical route, from reactants to products, tunneling through an activation barrier. There have been experimental measures, calculations, and talk in the literature on the role tunneling plays in catalyzed H atom transfer.[11−15] But, we feel, as of yet, tunneling in such reactions has not been carefully defined. Consider the following scenario: An experimentalist follows the dynamics of H atom transfer for a short time and then deduces a first-order rate constant, for example, by fitting the short-time decay of reactant concentration to a decaying exponential. Can this rate constant be considered as the "rate of tunneling"? One might argue if the barrier is large enough, the H atom had no other way to get to products other than tunneling, and yes indeed the measured rate constant is representative of a tunneling rate. There is a problem with this argument. What barrier is "high enough" to preclude all other routes to product production other than tunneling? The usual argument is that a barrier is too high for over the barrier production if its energy is much greater than the average of the thermal distribution of initial H atom energies at the temperature at which the rate is measured. The problem with this argument is that the H atom can be prepared in a nonequilibrium state and is not distributed according to a Boltzmann distribution. There have been arguments in the literature, for example, that claim that enzymes could prepare reactants in the most advantageous way as to approach products.[16−18] For example, an enzyme can cause the transfer of electron density away from bonding or into antibonding orbitals involved in binding the H atom to a donor atom of a substrate. In this case the H-donor bond will elongate and weaken, resulting in an H atom that is no longer in an equilibrium state. This H atom is then described, at $t = 0$, by a wavepacket not at equilibrium. A classical H atom, at zero temperature, prepared with energy, E_0, has this single, definite value of energy. The more correct view is that the H atom is a quantum mechanical particle, and even at zero temperature, is represented by a wavepacket having a distribution of energies. Say the H atom must overcome an activation barrier of energy E_A to become products. The H atom wavepacket at time zero, particularly if it is prepared in a nonequilibrium state, can have energy components above the barrier as well as components below the barrier. The ensuing quantum dynamics of this reactive system contains two events, an above-the-barrier H atom transfer from the components of the wavepacket initially above the barrier at

* To whom correspondence should be addressed. E-mail: messinam@uncw.edu.

10.1021/ct800436u CCC: $40.75
Published on Web 02/12/2009

time zero and tunneling through the barrier caused by the below the barrier components of the initial wavepacket. In this scenario the initial, short-time, decay of reactants would be dominated by the faster, above the barrier event, and the deduced rate constant would have very little to do with tunneling.

In this work we demonstrate that there is a reasonable definition of a rate constant for tunneling alone in a reactive event involving an atom that can tunnel through an activation barrier. For such a separation of dynamics in a single reactive event there has to be a rigorous definition of "components" of an initial wavepacket above and below a reactive barrier. We take the philosophy here that if we decompose an initial wavepacket into two such components, these components must satisfy two criteria.

The first one is that these two components must evolve independently of one another. For example, if we decompose the initial reactant wavepacket into an above the barrier and a below the barrier component, the quantum dynamics of the below the barrier component, that is, the one that represents tunneling alone, should evolve independently of the other component. If this is the case, then we could indeed view the overall single reactive process as being composed of a tunneling event and an above the barrier route to product production. We will see that there is only one way to decompose an initial wavepacket into these two components where each component evolves independently of the other. This is to expand the initial reactive wavepacket in the eigenstates of the $\hat{H}$ operator governing the time evolution of the initial wavepacket in the time-dependent Schrödinger equation (TDSE).

The second criteria is that we must be able to extract, out of the quantum dynamics of the system, a time-evolving probability density for each event. We show that such a division is possible for the common and ubiquitous double-well reactive system and, thus, are able to extract out a rate constant for tunneling alone.

This paper is organized as follows. In section II, we discuss the theory. We describe how an initial, nonequilibrium, H atom wavepacket can be decomposed into above and below the barrier components. We show that for one, special, decomposition, the ensuing dynamics of the system is separable into a tunneling and an above the barrier component. We also show in section II how this special decomposition of the initial H atom wavepacket yields a way to extract out a rate constant for the transfer event that is due to tunneling alone. In section III, we describe numerical results. In section III, we also make the connection between the theory presented and experimental observable quantities in a kinetics experiment. We show that it may be possible for an experimentalist to extract out a rate constant for tunneling alone in an H transfer reaction, just from experimentally observable data. Finally, in section IV, we discuss the results and conclusions.

II. Theory

(a). Decomposition of an Initial Wavepacket. Consider a quantum mechanical particle, such as an H atom, moving in a single spatial dimension, x. For now we leave the potential energy of the system unspecified. We assume that the particle can undergo a "reaction" and transfer from a reactant-side to a product-side of a reaction profile. We assume that an activation barrier of energy, E_A, spatially divides the reactants and products from one another. The reactants and products are separated by a dividing point at $x = x^*$. Thus, if the particle is at positions $x < x^*$, it is considered reactant, and is considered product if the particle is at positions $x > x^*$.

A classical particle, prepared with an energy E_0 at a temperature of $T = 0$ has a single, definite value of energy of E_0. Thus, if this classical particle has $E_0 > E_A$, it would have enough energy to overcome the activation barrier, allowing a reaction to occur. If $E_0 < E_A$, then the particle would not have enough energy to overcome the activation barrier and no reaction would take place.

The situation is more complicated if we treat the particle correctly, according to quantum mechanics. Say the particle, prepared at time, $t = 0$, is in a nonequilibrium state on the reactant side of the reaction, and is represented by a wave function, $\Psi_0(x,t=0)$. A particle represented by such a wave function does not have a single value of energy, but rather a distribution of energies, $P(E)$. For example, the probability of the particle having the activation energy is $P(E_A)$. The wavepacket, $\Psi_0(x,t=0)$, contains some energy values greater than E_A and others that are less than E_A. The components with energy greater than E_A have enough energy to overcome the activation barrier. Thus, the components of the initial wavepacket with $E > E_A$ do not get to products via tunneling but become products much as a classical particle would. If we want to ascribe a rate of reaction caused by tunneling alone, we must be careful to exclude these components of the initial wave function from consideration. The components of the initial reactant wavepacket with energy less than E_A, on the other hand, can only become products via tunneling and are the components of the initial wavepacket that contribute to the portion of the reaction rate caused by tunneling.

The initial wavepacket, $\Psi_0(x,t = 0)$, evolves in time according to the time-dependent Schrödinger equation (TDSE). At time, t, the wavepacket evolves into $\Psi(x,t)$, and the probability of the particle being on the reactant side of the barrier at this time is defined as $P_R(t)$ shown below

$$P_R(t) = \int_{x=-\infty}^{x=x^*} |\Psi(x,t)|^2 dx \tag{1a}$$

If the reaction follows first-order kinetics $P_R(t)$ should decay exponentially according to

$$P_R(t) = e^{-\kappa t} \tag{1b}$$

A method for determining the rate constant, κ, is as follows: Evolve $\Psi_0(x,t=0)$, in time by solving the appropriate TDSE, compute $P_R(t)$ by using eq 1a, and then fit the results to an exponential according to eq 1b and extract out the value of the rate constant κ. The problem with this method is that the rate constant found using this approach would not only include the components of $\Psi_0(x,t = 0)$ that tunnel through the barrier; it would also include the components of $\Psi_0(x,t$

$= 0$) that can energetically overcome the barrier. Thus, the rate constant determined by such an algorithm would not represent the rate of tunneling alone, but a combination of tunneling and above-the-barrier dynamics. If one wants to extract out a rate constant from the quantum dynamics just from tunneling another algorithm must be used.

What we have in mind is the decomposition of the initial reactant wavepacket into two components; $\Psi_0^-(x,t=0)$, the component of initial wavepacket below, and $\Psi_0^+(x,t=0)$, the component of initial wavepacket above the barrier, at $t = 0$. We then decompose the initial wavepacket as

$$\Psi_0(x,t=0) = \Psi_0^+(x,t=0) + \Psi_0^-(x,t=0) \tag{2}$$

The initial wavepackets $\Psi_0^-(x,t=0)$ and $\Psi_0^+(x,t=0)$ evolve according to the TDSE into $\Psi^-(x,t)$ and $\Psi^+(x,t)$, respectively. We want to be able to assign two rates of product production, κ^- and κ^+, where κ^- is the rate of product production because of tunneling alone, and κ^+ is the rate of product production due to above the barrier product production. The only way for these rates to be well defined is if we could define two probability densities, $P_R^-(t)$ and $P_R^+(t)$ as shown below

$$P_R^-(t) = \int_{x=-\infty}^{x=x^*} |\Psi^-(x,t)|^2 dx \tag{3a}$$

$$P_R^+(t) = \int_{x=-\infty}^{x=x^*} |\Psi^+(x,t)|^2 dx \tag{3b}$$

Both $P_R^-(t)$ and $P_R^+(t)$ should be decreasing functions of time because they describe the loss of reactant. Our conjecture is that there should be a wide disparity in the time−decay between $P_R^-(t)$ and $P_R^+(t)$, with the loss of reactant through tunneling, $P_R^-(t)$, being the slower process. For example, if both $P_R^-(t)$ and $P_R^+(t)$ were each described by a single exponential decay then we could write

$$P_R^-(t) \propto e^{-\kappa^- t} \tag{4a}$$

$$P_R^+(t) \propto e^{-\kappa^+ t} \tag{4b}$$

where κ^- is the rate constant for product production via tunneling and κ^+ is the rate constant for over the barrier production of product. If our conjecture about the wide disparity between the decay of $P_R^-(t)$ and $P_R^+(t)$ were true, then we would find $\kappa^- \ll \kappa^+$. In the Numerical Results section, we will say more about the particular functional forms of $P_R^-(t)$ and $P_R^+(t)$.

We now explore if we can indeed decompose the quantum dynamics of the system into two events: a tunneling event and an above the barrier production event.

To show that such a partition of the quantum dynamics, as shown in eqs 3a−4a, is possible, we now specify the Hamiltonian operator, $\hat{H}$, for the system as

$$\hat{H} = \frac{-\hbar^2}{2m}\frac{d^2}{dx^2} + V^*(x) \tag{5}$$

where the first term is the kinetic energy operator and the second term is potential energy of the system. The set of eigenstates, $\{\varphi_n(x)\}$ of any $\hat{H}$ operator forms a complete set of states. Thus, the initial wavepacket, $\Psi_0(x,t=0)$, can be expanded in terms of this complete set according to

$$\Psi_0(x,t=0) = \sum_n c_n |\varphi_n(x)\rangle \tag{6}$$

In the above equation, the set of eigenstates, $\{\varphi_n(x)\}$ can be a set of solutions to *any* time-independent Schrodinger equation, and the basis coefficients, $\{c_n\}$, can be determined by the projections

$$c_n = \langle \varphi_n(x) | \Psi_0(x,t=0) \rangle \tag{7}$$

Thus, the $\{\varphi_n(x)\}$can be taken as the solutions of *any* time-independent Schrödinger equation

$$\hat{H}\varphi_n(x) = E_n \varphi_n(x) \tag{8}$$

where $\hat{H}$ is a Hamiltonian operator containing any potential energy function, $V(x)$ and the $\{E_n\}$ are the set of eigenenergies. Within this spectrum of eigenenergies are two subsets, one, $\{E^-\} = \{E_1, E_2, E_3, ..., E_m\}$, is the set of energies below the barrier, and the other, $\{E^+\} = \{E_{m+1}, E_{m+2}, ...\}$, is the subset containing energies above the barrier. We can expand each of the initial wave functions, $\Psi_0^-(x,t=0)$ and $\Psi_0^+(x,t=0)$in this set of eigenstates as

$$\Psi_0^-(x,t=0) = \sum_{j=1}^{m} c_j |\varphi_j(x)\rangle \tag{9a}$$

$$\Psi_0^+(x,t=0) = \sum_{j=m+1} c_j |\varphi_j(x)\rangle \tag{9b}$$

Now we come to an important juncture. If the $\hat{H}$ operator in eq 8 does not contain the potential energy, $V^*(x)$, of our system, then the energies, $\{E_n\}$, are not the eigenenergies of our system, and we would not be sure that the subset of energies $\{E^-\} = \{E_1, E_2, E_3, ..., E_m\}$ truly represent components of the initial reactant wave function that are below the barrier. We now show that if the initial wavepacket was expanded in a set of eigenstates that are not the eigenstates of the $V^*(x)$ potential, then the wavepackets $\Psi^-(x,t)$ and $\Psi^+(x,t)$ do not evolve independently of one another and the separation of the quantum dynamics into separate tunneling and nontunneling events would not make sense.

We now introduce a set of eigenfunctions, $\{\psi_n(x)\}$, which *are* eigenfunctions of the Hamiltonian operator, $\hat{H}$ for our system as described in eq 5. These eigenfunctions have an associated set of eigenenergies,$\{E_n\}$, that are the true eigenenergies of our system. We can then, unambiguously, decompose this spectrum of energies into two subsets: $\{E^-\} = \{E_1, E_2, ..., E_m\}$, the set of energies having values less than E_A, and $\{E^+\} = \{E_{m+1}, E_{m+2}, ...\}$, the set containing above the barrier energies. This allows us to truly decompose the initial wavepacket into above and below the barrier components as

$$\Psi_0^-(x,t=0) = \sum_{j=1}^{m} c_j |\psi_j(x)\rangle \tag{10a}$$

$$\Psi_0^+(x,t=0) = \sum_{j=m+1} c_j |\psi_j(x)\rangle \tag{10b}$$

Now we consider the time-evolution of the initially decomposed wavepacket. We write the wavepacket for all times as

$$\Psi(x,t) = \Psi^{-}(x,t) + \Psi^{+}(x,t) \tag{11}$$

This wavepacket evolves according to the TDSE shown below

$$\hat{H}\Psi(x,t) = i\hbar\frac{\partial\Psi(x,t)}{\partial t} \tag{12}$$

Substituting eq 11 into the TDSE in eq 12 results in

$$\hat{H}\{\Psi^{-}(x,t) + \Psi^{+}(x,t)\} = i\hbar\frac{\partial\{\Psi^{-}(x,t) + \Psi^{+}(x,t)\}}{\partial t} \tag{13}$$

If the time-evolution of our system is truly composed of two separate independent dynamic events, then each event should be governed by it's own TDSE. Thus, there should be a TDSE for the tunneling event and one for the above the barrier dynamics. With this in mind, we decompose eq 13 into the following equations

$$i\hbar\frac{\partial\Psi^{-}(x,t)}{\partial t} = \hat{H}\Psi^{-}(x,t) \tag{14a}$$

$$i\hbar\frac{\partial\Psi^{+}(x,t)}{\partial t} = \hat{H}\Psi^{+}(x,t) \tag{14b}$$

We now explore the separability of the quantum dynamics of the system into tunneling and above-the-barrier dynamical components for a general expansion of $\Psi_0(x,t = 0)$ in a general set of eigenfunctions, $\{\varphi_n(x)\}$, as in eq 6. We define the set of time-dependent basis coefficients corresponding to eigenfunctions with energies below and above the barrier as $\{c^{-}(t)\}$ and $\{c^{+}(t)\}$, respectively. We solve the TDSE by putting eq 6 into eq 13 to get

$$i\hbar\left\{\sum_{j=1}^{m}\dot{c}_j^{-}(t)|\varphi_j(x)\rangle + \sum_{j=m+1}\dot{c}_j^{+}(t)|\varphi_j(x)\rangle\right\} = \sum_{j=1}^{m}c_j^{-}(t)\hat{H}|\varphi_j(x)\rangle + \sum_{j=m+1}c_j^{+}(t)\hat{H}|\varphi_j(x)\rangle \tag{15}$$

Now we multiply eq 15 on the left by, $\varphi_{\ell}(x)$, an eigenfunction with an energy below the barrier, and then integrate over all space to get

$$i\hbar\dot{c}_{\ell}^{-}(t) = \sum_{j=1}^{m}c_j^{-}(t)H_{\ell j} + \sum_{j=m+1}c_j^{+}(t)H_{\ell j} \tag{16}$$

In eq 16, the Hamiltonian matrix elements, $H_{\ell j}$, are defined by

$$H_{\ell j} = \langle\varphi_{\ell}(x)|\hat{H}|\varphi_j(x)\rangle \tag{17}$$

According to eq 16, the time-evolution of $c_{\ell}^{-}(t)$, a basis coefficient governing the dynamical evolution of a wavepacket component below the barrier is not independent of the above the barrier components of the wave function, that is, $\Psi^{+}(x,t)$. This is because, as shown in eq 16, the differential equation governing below the barrier coefficients, $\{c^{-}(t)\}$, depends on above the barrier coefficients, $\{c^{+}(t)\}$. Thus, in a general expansion of the initial wavepacket in a general set of eigenstates, $\{\varphi_n(x)\}$, we cannot separate the dynamics into tunneling dynamics and above the barrier dynamics. Now we ask if such a separation of dynamics is possible if $\Psi_0(x,t = 0)$ is expanded in the special set of complete states, that is, $\{\psi_j(x)\}$, that are solutions of the TDSE with $V = V^*(x)$, that is, the potential energy of the system being studied. If we use these eigenstates as a basis, then the Hamiltonian matrix elements in eq (17) become

$$H_{\ell j} = \langle\psi_{\ell}(x)|\hat{H}|\psi_j(x)\rangle = \mathrm{E}_j\langle\psi_{\ell}(x)|\psi_j(x)\rangle = \mathrm{E}_j\cdot\delta_{\ell j} \tag{18}$$

Equation 16 then, in this case, becomes

$$\dot{c}_{\ell}(t) = -\frac{i}{\hbar}\mathrm{E}_{\ell}\cdot c_{\ell}(t) \tag{19}$$

A similar differential equation obtains, for all the basis coefficients, if we expand $\Psi^0(x,t = 0)$ in the set of eigenfunctions, $\{\psi_j(x)\}$, of our potential energy, $V^*(x)$. As shown in eq 19, each below the barrier coefficient, $c_{\ell}(t)$, evolves independently of all the others, and most importantly, independently of the above the barrier coefficients, $\{c^{+}(t)\}$. This demonstrates that tunneling and over-the-barrier quantum dynamics can be considered separately if we expand $\Psi_0(x,t = 0)$ in the set of eigenfunctions of the $\hat{H}$ operator, that is, in the set $\{\psi_j(x)\}$. Within this expansion the basis coefficients evolve according to

$$c_{\ell}(t) = c_{\ell,0}\cdot\mathrm{e}^{-\frac{i}{\hbar}\mathrm{E}_{\ell}t} \tag{20a}$$

where the initial value of the basis coefficients, $c_{\ell,0}$, are calculated from

$$c_{\ell,0} = \langle\psi_{\ell}(x)|\Psi^0(x,t=0)\rangle \tag{20b}$$

Thus far we have shown that the quantum dynamics of a "reactive" system can be separated into two dynamic events: tunneling and above the barrier transfer. We have also shown that this separation is only obtained if the initial wavepacket is decomposed in terms of the eigenstates of the system of interest. We have *not* yet demonstrated that the total time evolution of the probability density, $P_{\mathrm{R,T}}(t)$, can be broken up into two pieces as suggested by eqs 3b−4b. This must be the case if we are to be able to ascribe a rate solely for tunneling in a reaction. The total probability density of reactant at a time t is given by

$$P_{\mathrm{R,T}}(t) = \int_{x=-\infty}^{x=x^*}|\Psi(x,t)|^2\mathrm{d}x = \int_{x=-\infty}^{x=x^*}|\Psi^{-}(x,t) + \Psi^{+}(x,t)|^2 \tag{21}$$

The second equality comes from the definition of the wavepacket, $\Psi(x,t)$, in eq 11. We then expand out the square in eq 21. Using the definition for the separate probability densities given by eqs 3a, we can then write eq 21 as

$$P_{\mathrm{R,T}}(t) = P_{\mathrm{R}}^{-}(t) + P_{\mathrm{R}}^{+}(t) + 2\cdot\mathrm{Re}\left[\int_{x=-\infty}^{x=x^*}\Psi^{-}(x,t)\cdot\Psi^{+}(x,t)\right] \tag{22}$$

Thus, the definition of two probability densities, one for tunneling, and one for above the barrier transfer, will only be true if the last term in eq 22 is zero, or nearly so. To show that this is indeed the case we now discuss the potential energy under consideration here in more detail.

(b). Double-Well Potential. The double-well potential, is by far, the most commonly used potential energy surface used to describe the transfer of an atom from one moiety to another.[19,20] We consider a double-well potential as naturally

arising from two diabatic states. We consider here a double-well potential built out of two harmonic single-dimensional diabatic states, a reactant state, $V_R(x)$, and a product state, $V_P(x)$. These diabatic states are defined below

$$V_R(x) = \frac{m\omega_R^2}{2}(x - x_R^0)^2 \tag{23a}$$

and

$$V_P(x) = \frac{m\omega_P^2}{2}(x - x_P^0)^2 \tag{23b}$$

Here $\{\omega_R,\omega_P\}$are the frequencies of the reactant and product wells, respectively, and $\{x_R^0,x_P^0\}$ are the minima of the wells. These diabatic states are coupled to one another via a coupling function, $g(x)$, given by

$$g(x) = g_0 \cdot e^{-\alpha(x-x^*)^2} \tag{24}$$

The degree of coupling between the states is set by the coupling strength, g_0, and the maximum coupling occurs at the dividing point between reactants and products, x^*. Thus, we take the dividing line between reactants and products as the value of position x^* lying between the two minima,$\{x_R^0,x_P^0\}$, and making $V_R(x^*) = V_P(x^*)$. The length scale of the coupling is set by α. If α is large the coupling between the states becomes more localized around the crossing point, x^*.

A well-known, and useful approximation, to the diabatic system described above is it is adiabatic, double-well analogue.[20] In this approximation, there is a single wavepacket describing the evolution of the system, $\Psi(x,t)$, which evolves on a single adiabatic potential, $V^*(x)$. This adiabatic potential is taken as the lowest eigenvalue of the potential energy matrix

$$\underset{\approx}{V} = \begin{bmatrix} V_R(x) & g(x) \\ g(x) & V_P(x) \end{bmatrix} \tag{25}$$

This lowest eigenvalue describes a double-well potential and is given by

$$V^*(x) = \frac{V_R(x) + V_P(x)}{2} - \frac{\sqrt{[V_R(x) - V_P(x]^2 + 4 \cdot g(x)^2}}{2} \tag{26}$$

The quantum dynamics of this system is fully described by a single, time-evolving wavepacket, $\Psi(x,t)$, that evolves according to the TDSE

$$i\hbar\frac{\partial\Psi(x,t)}{\partial t} = [\hat{T} + V^*(x)] \cdot \Psi(x,t) \tag{27}$$

The initial adiabatic wavepacket is given by, $\Psi(x,t=0) = \Psi_0(x,t=0)$, where $\Psi_0(x,t=0)$ is a wavepacket localized in the reactant well, that is, having it's maximum near to $x = x_R^0$. This initial wavepacket can be decomposed into above and below the barrier components, as described above, by expanding it in the set of eigenfunctions of the time-independent Schrödinger equation below

$$[\hat{T} + V^*(x)] \cdot \Psi(x) = \mathrm{E} \cdot \Psi(x) \tag{28}$$

(c). Separation of the Probability Densities. We still have to show that the definition of two probability densities, that is, $P_R^-(t)$ for tunneling production and $P_R^+(t)$ for above the barrier production of products makes sense. Above we have shown that we can indeed ascribe two separate probability densities for the dynamics of each event if eq 22 is true, that is, if the last term on the RHS is zero, or nearly so.

It is well-known, that in a double well system as described here, the eigenstates come in pairs. Each pair is composed (approximately) of a plus and minus combination of the eigenstates of $V_R(x)$ and $V_P(x)$. Specifically, we can write the eigenstates of or system as

$$\psi_{2j+1}(x) \approx c_{2j+1}\{|R_j\rangle + |P_j\rangle\} \quad j = 0, 1, 2, ... \tag{29a}$$

and

$$\psi_{2j}(x) \approx c_{2j}\{|R_{j-1}\rangle - |P_{j-1}\rangle\} \quad j = 1, 2, 3, ... \tag{29b}$$

Here $\{|R_j\rangle,|P_j\rangle\}$are the eigenstates of $V_R(x)$ and $V_P(x)$, respectively. [Note these are harmonic oscillator eigenstates, whose index conventionally starts at $j = 0$.] The $|R_j\rangle$ eigenstates are localized on the reactant side of the double-well potential, and the $|P_j\rangle$ eigenstates are localized in the product well and are nearly zero in the region $x = -\infty \rightarrow x^*$. Since the integral in eq 22 runs from $x = -\infty \rightarrow x^*$, that is, the portion of space where the $|P_j\rangle$ components of the$\{\psi_j(x)\}$are nearly zero we can define components of $\Psi^+(x,t)$ and $\Psi^-(x,t)$ that contribute to the integral in eq 22 as $\chi^+(x,t)$ and $\chi^-(x,t)$ as shown below

$$\chi^-(x,t) = \sum_{j=0}^{m}(c_{2j+1} + c_{2j+2}) \cdot |R_j(x)\rangle \tag{30a}$$

and

$$\chi^+(x,t) = \sum_{\ell=m+1}^{m}(c_{2\ell+1} + c_{2\ell+2}) \cdot |R_\ell(x)\rangle \tag{30b}$$

The integral in eq 22 then becomes

$$\int_{x=-\infty}^{x=x^*}[\Psi^-(x,t)]^* \cdot \Psi^+(x,t)\mathrm{d}x \approx \int_{x=-\infty}^{x=x^*}[\chi^-(x,t)]^* \cdot \chi^+(x,t)\mathrm{d}x \tag{31}$$

Substitution of eq 30a into eq 31 shows that the integral in eq 22 is composed of a sum of terms of the form $\int_{x=-\infty}^{x=x^*}R_j(x) \cdot R_l(x)\,\mathrm{d}x$ with $j \neq \ell$ in each case. Since the $|R_j\rangle$ eigenstates are nearly orthogonal over this interval, the integral in eq 31 and, hence, the one in eq 22 are nearly zero. This means that the separation of the evolved probability densities into a tunneling and above the barrier probability density can be achieved. There are two important points to make about this argument. First, the last term on the RHS of eq 22 is only very small if the initial wavepacket, $\Psi_0(x,t = 0)$, is expanded in the exact eigenstates of the double-well system, $\{\psi_j(x)\}$. Second, there is one case where eq 22 will not be even approximately true. This is the case where the plus eigenstate $|R_j\rangle + |P_j\rangle$ is below the barrier and its companion $|R_j\rangle - |P_j\rangle$ is above. In this case, there will be a large contribution to the integral from a term of the form $\int_{x=-\infty}^{x=x^*}R_j(x) \cdot R_l(x)\,\mathrm{d}x$ with $j = \ell$, which is not zero and is in fact approximately unity. But, in all cases studied, we have

not found a case where this situation occurs. Thus, we feel that this happens rarely enough to be neglected.

III. Numerical Results

For all calculations we use the lower adiabatic, double-well, potential given by $V^*(x)$ in eq 26. Some parameters are constant throughout the calculations and we discuss these first. Since we plan to focus on tunneling, we choose the mass of the system, m, to be that of an H atom, m_H. We also explore the isotope effect on the tunneling dynamics by setting the system mass to that of a Deuteron in some calculations, in these cases $m = 2m_H$. The minima of the reactant and product wells, that is, x_R^0 and x_P^0, in eqs 25−26 are 3.0 and 4.25 Å, respectively. Thus, in all calculations the distance between the well minima is 1.25 Å. The frequency of the product well, ω_P, is $\omega_P = 2000$ cm^{-1} in all calculations. We take the length scale of the nonadiabatic coupling, α, to be 1.0 Å^{-2} in all calculations. Some parameters are varied to explore their effect on the quantum dynamics of the system. The reactant well frequency, ω_p, varies between 1500 and 2000 cm^{-1}. The nonadiabatic coupling strength, g_0, is varied between 100 and 220 kJ mol^{-1}. These coupling strengths result in barrier heights, E_A, ranging between 45 and 125 kJ mol^{-1}.

The eigenstates, $\{\psi_j\}$, of the double-well potential are calculated by using a particle in a box basis set. The spatial grid runs from $x = 0$ Å $\rightarrow x = 6$ Å, with 256 equally spaced grid points. In all calculations the results converged with a basis set comprised of 100 basis functions.

The initial wavepacket of the system, $\Psi_0(x,t = 0)$, is localized on the reactant side of the potential and is taken as the Gaussian shown below

$$\Psi_0(x, t=0) = \left(\frac{m\omega_0}{\pi\hbar}\right)^{\frac{1}{4}} \cdot \exp\left\{-\left(\frac{m\omega_0}{2\hbar}\right) \cdot [x - (x_R^0 - \delta x)]^2\right\} \quad (32)$$

The width of the initial wavepacket is set by the frequency, ω_0, which we take as 2000 cm^{-1} in all calculations. The initial displacement of the wavepacket from equilibrium is controlled by the parameter δx in eq 32. If $\delta x = 0$, then the wavepacket is centered at its equilibrium position at $t = 0$ in the reactant well. As δx increases the initial reactant wavepacket is displaced more from equilibrium and, thus, possesses more initial energy.

As described previously, this initial wavepacket is then expressed as a superposition of the eigenstates of the system, that is, $\{\psi_j\}$, and further broken down into below and above the barrier components as described in eqs 2, 9a and 9b. We chose to study a system where there is no chance for reactant that has crossed the dividing point $x = x^*$ to recross and go back toward reactants. To do this we need a mechanism for pulling probability density off of the product well. We cannot do this by evolving the basis coefficients as shown in eq 20a. We carry this out by discretizing the initial wavepackets on a spatial grid and solving the TDSEs in eqs 14a and 14b via the Feit−Fleck split operator technique. We are then able to pull probability density off of the product state by setting $\Psi(x,t) = 0$ for all $x > x_P^0$

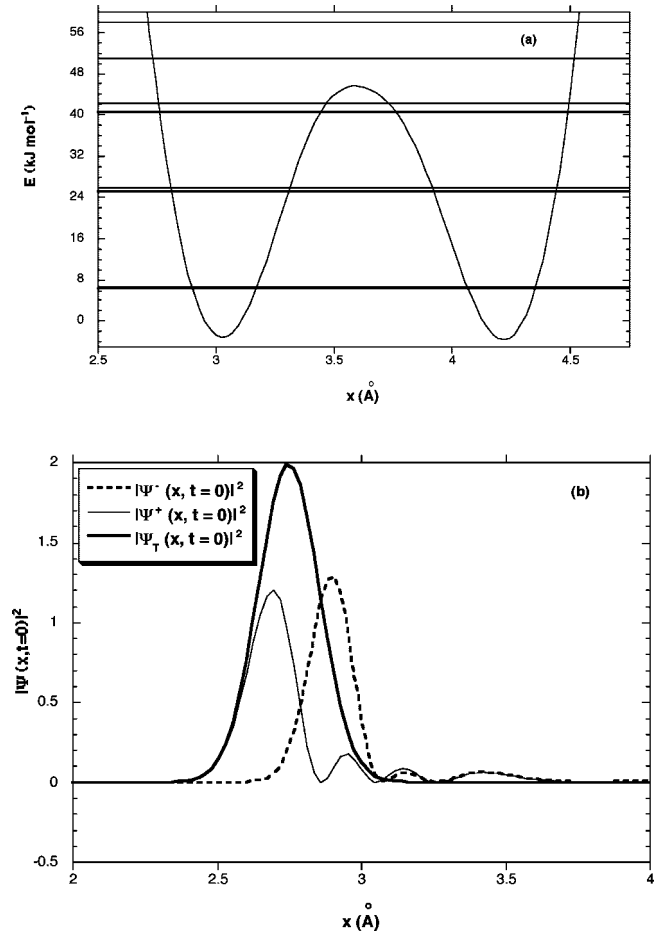

Figure 1. (a) Double-well potential when $\omega_R = \omega_P = 2000$ cm^{-1} with a nonadiabatic coupling strength of $g_0 = 230$ kJ mol^{-1}. The eigenenergies of this system, $\{E\}$, are shown as horizontal lines inside the potential. (b) The squares of the initial wave function and it is below and above the barrier components as described in the text with the thick solid line as the total wave function, the thick dashed line as the below the barrier component and the thin solid as the above the barrier component.

during the course of the time-evolution of the wavepackets. For all calculations in which we solve the TDSE, the spatial grid is the same as that for the basis set calculations and the time step is d$t = 0.01$ fs.

In Figure 1a, we show the double-well potential when $\omega_R = \omega_P = 2000$ cm^{-1} with a nonadiabatic coupling strength of $g_0 = 230$ kJ mol^{-1}. This leads to a double-well potential with a barrier height of $E_A = 45$ kJ mol^{-1}, which is the lowest barrier considered. The eigenenergies of this system, $\{E\}$, are shown as horizontal lines inside the potential. There are 6 eigenstates below the barrier, and as described above, they come in pairs of two. All the other eigenenergies that are above the barrier are no longer paired as those below.

In Figure 1b, we show the initial wave function and its below and above the barrier components when the initial wave function is displaced by an amount $\delta x = 0.25$ Å from equilibrium at $t = 0$. The thick solid line in Figure 1b is the square of the total wave function, $\Psi_0(x,t = 0)$, which is centered at position $x_R^0 - \delta x = 2.75$ Å. The thick dashed line is the square of the below the barrier component of the initial wave function, $\Psi_0^-(x,t = 0)$, of the initial wave

function. The thin solid line in Figure 1b is the square of the above the barrier component, $\Psi_0^+(x,t=0)$, of the initial wave function. Note that the more energetic above the barrier component has more nodes than the below the barrier component, which is consistent with it being the more energetic component. Further, the maximum of the above the barrier wavepacket, $\Psi_0^+(x,t=0)$, occurs at $x \approx 2.6$ Å, which is 0.4 Å from equilibrium. The maximum of the below the barrier component, on the other hand, occurs at $x \approx 3.0$ Å, which is where the equilibrium of the reactant well occurs. Thus, the component of the wave function that is responsible for product production through tunneling is that component of the initial reactant wavepacket that is nearly at equilibrium on the reactant state.

We now consider the ensuing quantum dynamics of this initially displaced wavepacket. We express this wavepacket as a superposition of the double-well eigenstates and form $\Psi_0^-(x,t=0)$ and $\Psi_0^+(x,t=0)$ according to eqs 10a and 10b. We can determine how much of the wavepacket is above and below the barrier at $t = 0$, that is, $P_R^-(t=0)$ and $P_R^+(t=0)$, respectively, from

$$P_R^-(t=0) = \int_{-\infty}^{+\infty} |\Psi_0^-(x,t=0)|^2 \cdot dx \tag{33a}$$

and

$$P_R^+(t=0) = \int_{-\infty}^{+\infty} |\Psi_0^+(x,t=0)|^2 \cdot dx \tag{33b}$$

With an initial displacement of the wavepacket of $\delta x = 0.25$ Å $P_R^-(t=0) = 0.5$ and $P_R^+(t=0) = 0.5$. Thus, in this case half the initial wavepacket contains energy components above the barrier. We then evolve $\Psi_0^-(x,t=0)$ and $\Psi_0^+(x,t=0)$ in time according to eqs 14a and 14b using the Feit−Fleck operator algorithm,[21] and in Figure 2a, we show the evolution of the total reactant probability density, $P_{R,T}(t)$. The solid line is approximation to the total reactant probability density obtained when we separate it into it is $P_R^-(t)$ and $P_R^+(t)$ components and set $P_{R,T}(t) \approx P_R^-(t) + P_R^+(t)$. The dashed line in Figure 2a is the exact total reactant probability density. We obtain this probability density by evolving the whole of the initial wavepacket, $\Psi_0(x,t=0)$, in time according to the TDSE in eq 12. The close agreement between the solid and dashed lines shows that, indeed, in this case the total reactant probability density can be split up into its below and above the barrier components. In fact, we have found that this was the case in all calculations we have performed. Although it may not be obvious from Figure 2a, the time-evolution of the reactant probability density does not follow a single decaying exponential.

Again, we assume that there is a large separation between the time scales of tunneling and over the barrier production. We still need to choose particular functional forms for $P_R^-(t)$ and $P_R^+(t)$ to quantify these time scales. For simplicity, we take both $P_R^-(t)$ and $P_R^+(t)$ as being described by an exponential decay as described in eq 4a. It is important to keep in mind that we have offered no proof that each of $P_R^-(t)$ and $P_R^+(t)$ should be exactly represented by a single exponential decay. In fact, if each below the barrier eigenstate decayed exponentially then the aggregate decay because of tunneling, $P_R^-(t)$, should not be exactly represented by a single decaying exponential but rather by a sum of decaying exponentials. We are assuming that a *comparison* of the two dynamic events, that is, tunneling and over the barrier production, could be well quantified by treating both events as first order events. The following numerical results will demonstrate that this assumption has some validity.

The thicker solid line in Figure 2a shows the best single exponential fit of $P_{R,T}(t)$. In Figure 2b, we show the evolution of the below the barrier component of the wavepacket, that is, $P_R^-(t)$. This probability density represents what we are claiming is the tunneling dynamics of the system. The thicker solid line in Figure 2b shows the best fit to $P_R^-(t)$ to a single, decaying, exponential. The tunneling dynamics alone fits a single exponential decay much more closely than that of the whole time evolution of the probability density. We extract out a rate constant for tunneling from the exponential fit in Figure 2b according to eq 4a and find, in this case, $\kappa^- = 7.5 \times 10^{-6}$ au. In Figure 2c, we show the evolution of the above the barrier probability density, that is, $P_R^+(t)$. The thick solid line in Figure 2c shows the best single decaying exponential fit to $P_R^+(t)$. Although the single exponential fit of $P_R^+(t)$ is not as good as that of $P_R^-(t)$ the fit does follow the overall decay trend pretty well. We extract out a rate constant for above the barrier product production from the exponential fit in Figure 2c according to eq 4b and find, in this case, $\kappa^+ = 5.3 \times 10^{-4}$ au. There is a large separation of time scales between the product production through tunneling, that is, κ^-, and the above the barrier production, that is, κ^+. In this case, in fact, there is a 2 orders of magnitude difference, with the tunneling being the slower process.

Now lets discuss the results in Figure 2 from an experimental viewpoint. The only observable that an experimentalist can measure is the total reactant probability density, that is, $P_{R,T}(t)$. If an experimentalist follows the decay of reactant concentration they would generate a concentration versus time profile like that shown by the thin solid line in Figure 2a. We have shown that this time profile results from two different dynamic routes toward product production: tunneling and above the barrier production. Further, the separation in time scales of these two events is very large. Thus, how can an experimentalist go from a measured concentration versus time profile like that in Figure 2a and extract out a "tunneling rate"? We offer an answer here.

We have shown that the total probability density, at least for a double-well potential, can be written as a sum of two distinct probability densities: $P_{R,T}(t) \approx P_R^-(t) + P_R^-(t)$. Thus, if both of the dynamic events, tunneling and above the barrier production are first-order events then each of $P_R^-(t)$ and $P_R^+(t)$ will decay exponentially and perhaps we can write the overall decay of the reactant concentration in time as

$$P_{R,T}(t) = P_R^-(0) \cdot e^{-\kappa^- t} + P_R^+(0) \cdot e^{-\kappa^+ t} \tag{34}$$

Here, $\{P_R^-(0), P_R^+(0)\}$ are the below and the above the barrier probability densities contained in the initial wavepacket as described in eqs 33a and 33b. The two rate constants, $\{\kappa^-, \kappa^+\}$, are the rate constants for product production through tunneling and above the barrier transfer, respectively. Thus, we are claiming that the overall decay of the reactant concentration should follow, at least approximately, a biex-

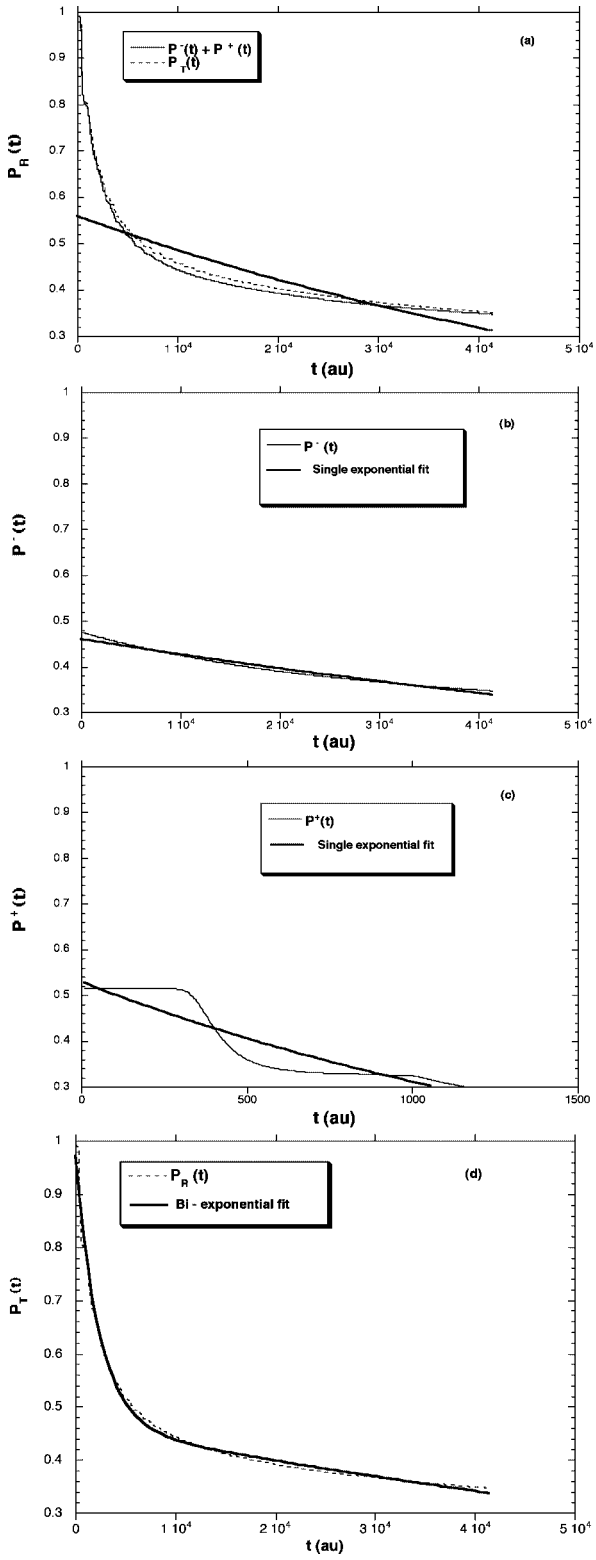

Figure 2. Evolution of the reactant probability density, $P_R(t)$, in the potential energy shown in Figure 1(a) and an initial displacement of $\delta x = 0.25$ Å: (a) the exact total reactant probability density (dashed line) and the approximate probability density (thin solid line). The thicker solid line shows the best single exponential fit of $P_{R,T}(t)$. (b) The evolution of the below the barrier probability density, $P_R^-(t)$ (thin solid line), and the best single exponential fit (thick solid line). (c) Evolution of the above the barrier probability density, that is, $P_R^+(t)$ (thin solid line), and the best exponential fit (thick solid line). (d) The biexponential fit to the reactant probability density, $P_R(t)$ (thick solid line), and the exact total reactant probability density (dashed line).

ponential decay. To explore the validity of this claim we fit the decay of the total reactant probability, $P_{R,T}(t)$, to a biexponential of the form

$$P_{R,T}(t) = a_0 \cdot e^{-a_1 t} + b_0 \cdot e^{-b_1 t} \tag{35}$$

using the Levenberg−Marquardt algorithm.[22] In performing this fit, we did *not* use initial guesses that reflect the fact that $a_0 = P_R^-(0)$ and $b_0 = P_R^+(0)$. This is because an experimentalist would not know this information; all they know is the observed total decay of the reactant concentration in time. In all calculations we use the initial guesses for the fit parameters of $a_0 = a_1 = b_0 = b_1 = 0.1$. In Figure 2d, we show the biexponential fit to the $P_{R,T}(t)$ in Figure 2a. The solid line is the fit, and the dashed line is the decay of total reactant probability density. As shown by Figure 2d, the time profile $P_{R,T}(t)$ is fit extremely well with a biexponential decay. In this fit, the parameters in eq 35 were as follows: $a_0 = 0.5$ au, $a_1 = 7.7 \times 10^{-6}$ au, $b_0 = 0.5$ au, $b_1 = 4.3 \times 10^{-4}$ au. A comparison of eqs 34 and 35 shows that $\{a_1,b_1\} = \{\kappa^-,\kappa^+\}$, and $\{a_0,b_0\} = \{P_R^-(0),P_R^+(0)\}$. As shown in Figure 2b, the tunneling rate constant was found to be $\kappa^- = 7.5 \times 10^{-6}$ au, which compares very favorably to the biexponential fit parameter, $a_1 = 7.7 \times 10^{-6}$ au. The over the barrier rate constant found from the single exponential fit in Figure 2c was $\kappa^+ = 5.3 \times 10^{-4}$ au, which compares very favorably to the biexponential fit parameter, $b_1 = 4.3 \times 10^{-4}$ au. Finally, as described above, for the case represented by Figures (2) the initial probability densities were $\{P_R^-(0),P_R^+(0)\} = \{0.5,0.5\}$, which compares very favorably to the fit parameter values of $\{a_0,b_0\} = \{0.5,0.5\}$.

In Figure 3, we show results for the same case as Figure 2, but now the initial wavepacket is displaced by an amount $\delta x = 0.10$ Å from equilibrium at $t = 0$. With this initial displacement of the wavepacket, $P_R^-(t = 0) = 0.935$ and $P_R^+(t = 0) = 0.065$. Thus, in this case only ~5% of the initial wavepacket contains energy components above the barrier. In Figure 3a, we show the decay of the total reactant probability density in time with the dashed line. The solid line is the best biexponential fit to $P_{R,T}(t)$. The parameters from the fit lead to the values for the two rate constants of $\kappa^- = 1.5 \times 10^{-6}$ au for the tunneling rate and $\kappa^+ = 2.1 \times 10^{-4}$ au for the above the barrier rate. In Figure 3b, we show the time evolution of the $P_R^-(t)$ probability density with a solid line. The dashed line in Figure 3b is the best single exponential fit which leads to another value for the tunneling rate constant: $\kappa^- = 1.8 \times 10^{-6}$ au. Again, an experimentalist can only observe the data reflected in Figure 3a, that is, the time evolution of $P_{R,T}(t)$. From the observable data along with a biexponential fit the experimentalist would conclude that the tunneling rate is $\kappa^- = 1.5 \times 10^{-6}$ au, which is in very good agreement to the actual rate of tunneling from the unobservable, but theoretically calculated value of $\kappa^- = 1.8 \times 10^{-6}$ au. In Figure 3c, we show the time evolution of the above the barrier probability density, $P_R^+(t)$ (thin line). The thick solid line is the best single exponential fit to $P_R^+(t)$, which leads to another value of κ^+ of $\kappa^+ = 1.6 \times 10^{-4}$ au, which compares favorably to the rate extracted from the experimentally realizable data of $\kappa^+ = 2.1 \times 10^{-4}$ au.

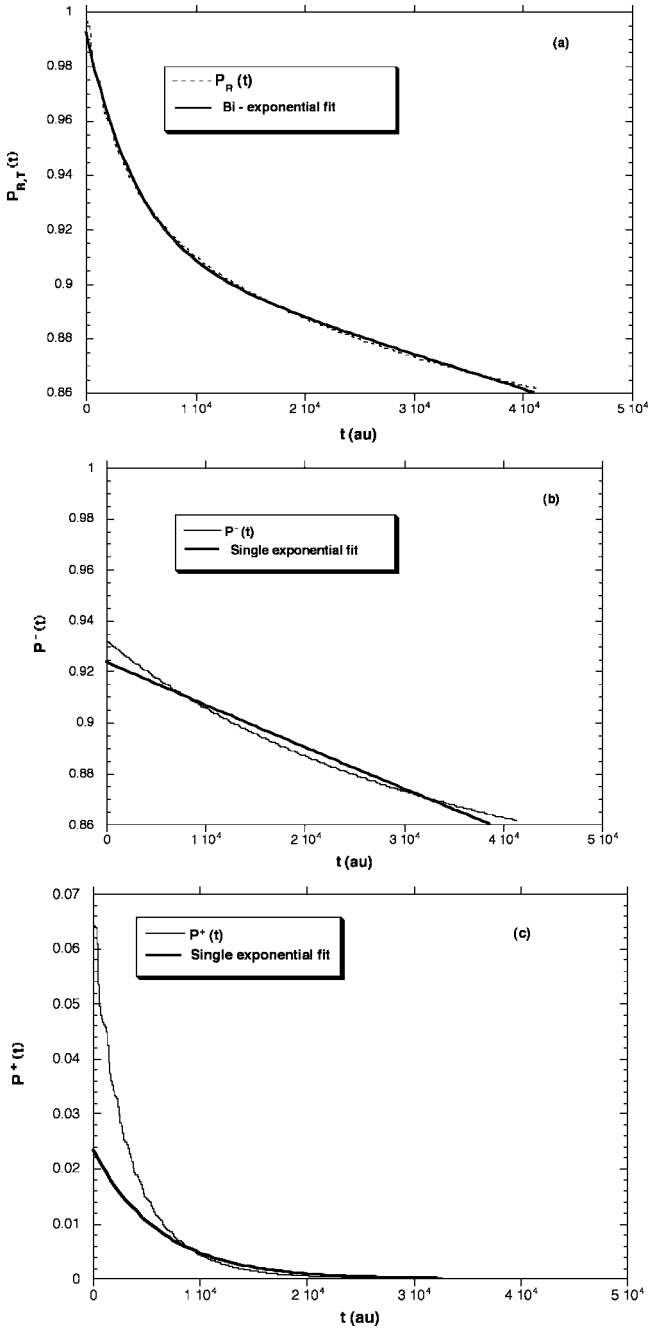

Figure 3. The evolution of the reactant probability density, $P_R(t)$ in the potential energy shown in Figure 1a and an initial displacement of $\delta x = 0.10$ Å: (a) the exact total reactant probability density (dashed line), and the biexponential fit (solid line). (b) The evolution of the below the barrier probability density, $P_R^-(t)$ (thin solid line) and the best single exponential fit (thick solid line). (c) Evolution of the above the barrier probability density, that is, $P_R^+(t)$ (thin solid line) and the best exponential fit (thick solid line).

Next, we explore if the claims above hold for systems with a larger barrier between the reactants and products. In Figures 4 and 5, we show results for a system with potential parameters of $\omega_R = \omega_P = 2000$ cm^{-1} and a nonadiabatic coupling strength of $g_0 = 150$ kJ mol^{-1}. This leads to a double well potential with a barrier height of $E_A = 125$ kJ mol^{-1}. In this case 12 eigenstates are below the barrier, and as described above, they come in pairs of two. In Figure 4,

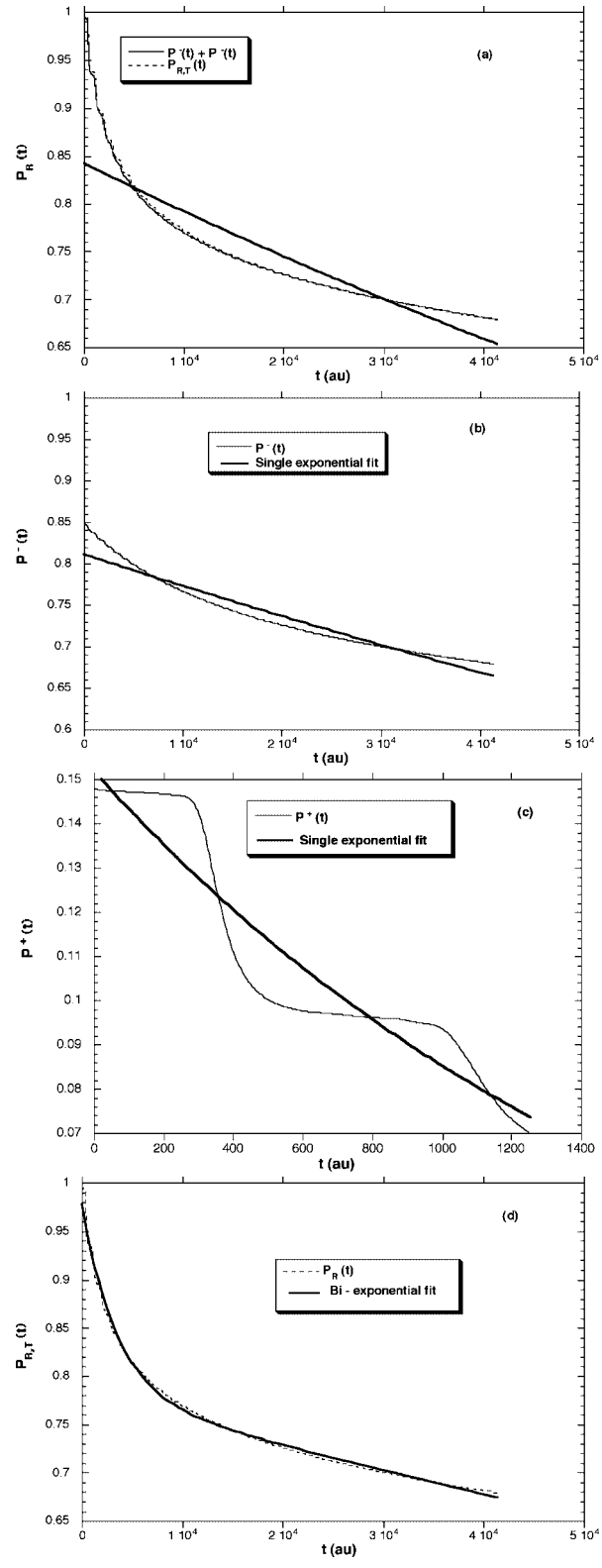

Figure 4. Evolution of the reactant probability density, $P_R(t)$, in a double-well potential with a barrier height of 125 kJ mol^{-1} and an initial displacement of $\delta x = 0.30$ Å: (a) the exact total reactant probability density (dashed line), the approximate probability density (thin solid line). The thicker solid line shows the best single exponential fit of $P_{R,T}(t)$. (b) The evolution of the below the barrier probability density, $P_R^-(t)$ (thin solid line) and the best single exponential fit (thick solid line). (c) Evolution of the above the barrier probability density, that is, $P_R^+(t)$ (thin solid line) and the best exponential fit (thick solid line). (d) The biexponential fit to the reactant probability density, $P_R(t)$, (solid line) and the exact total reactant probability density (dashed line).

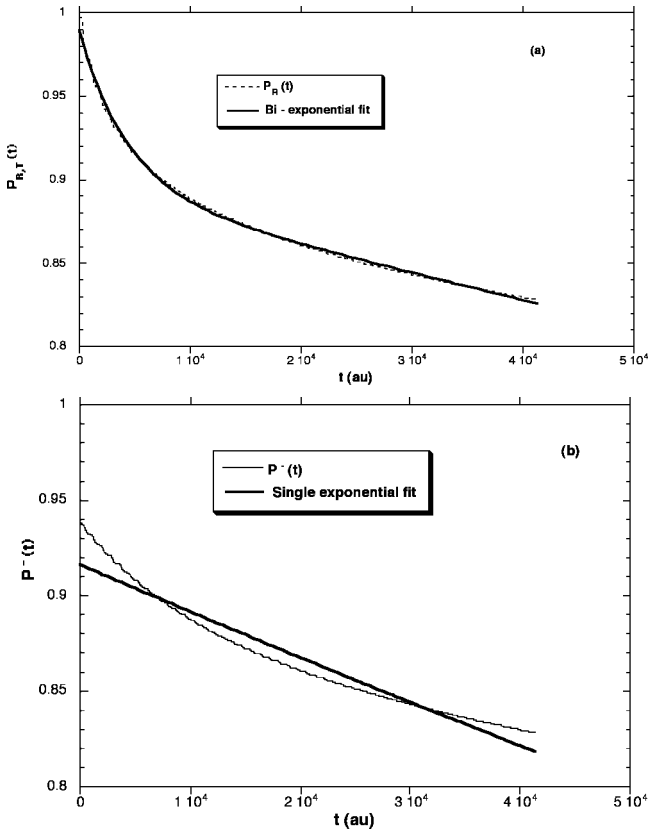

Figure 5. Evolution of the reactant probability density, $P_R(t)$, in a double-well potential with a barrier height of 125 kJ mol^{-1} and an initial displacement of $\delta x = 0.25$ Å: (a) the exact total reactant probability density (dashed line) and the biexponential fit (solid line). (b) The evolution of the below the barrier probability density, $P_R^-(t)$ (thin solid line) and the best single exponential fit (thick solid line).

we show results when the initial reactant wavepacket is displaced by an amount $\delta x = 0.3$ Å from equilibrium at $t = 0$. With this displacement and this potential, the initial below and above the barrier probability densities are $P_R^-(t = 0) = 0.85$ and $P_R^+(t = 0) = 0.15$, respectively. In Figure 4a, we show the evolution of the total reactant probability density, $P_{R,T}(t)$. The thin solid line is approximation to the total reactant probability density obtained when we separate it into it's $P_R^-(t)$ and $P_R^+(t)$ components and the dashed line in Figure 4a is the exact total reactant probability density. Because the thin solid and dashed lines are in close agreement, the dynamics of the system is separable into below and above the barrier probability densities even with a larger barrier. The thicker solid line in Figure 4a shows the best single exponential fit to the data, which is poor. In Figure 4b, we show the evolution of the below the barrier component of the wavepacket, that is, $P_R^-(t)$ (thin line). The thick line in Figure 4b shows the best fit of $P_R^-(t)$ to a single, decaying, exponential. Again, the tunneling dynamics alone fits a single exponential decay much more closely than that of the whole time evolution of the probability density. We extract out a rate constant for tunneling from the exponential fit in Figure 4b and find, in this case, $\kappa^- = 4.8 \times 10^{-6}$ au. The thin line in Figure 4c is the evolution of the above the barrier probability density, that is, $P_R^+(t)$. The thick line in Figure 4c shows the best single decaying exponential fit to $P_R^+(t)$. We extract out a rate constant for above the barrier product production from the exponential fit in Figure 4c and find, in this case, $\kappa^+ = 4.3 \times 10^{-4}$ au. In Figure 4d, we show the decay of the total reactant probability density in time with the dashed line. The solid line is the best biexponential fit to $P_{R,T}(t)$. The parameters from the fit lead to the values for the two rate constants of $\kappa^- = 3.6 \times 10^{-6}$ au for the tunneling rate and $\kappa^+ = 3.0 \times 10^{-4}$ au for the above the barrier rate. Again, these values represent information that can be extracted from the experimentally observable total rate of decay of reactant concentration. These values compare favorably with calculated separate tunneling and above the barrier rates of $\kappa^- = 4.8 \times 10^{-6}$ au and $\kappa^+ = 4.3 \times 10^{-4}$ au, respectively.

In Figure 5, we show results when the initial reactant wavepacket is displaced by an amount $\delta x = 0.25$ Å from equilibrium at $t = 0$. With this displacement and this potential, the initial below and above the barrier probability densities are $P_R^-(t = 0) = 0.95$ and $P_R^+(t = 0) = 0.05$, respectively. In Figure 5a, we show the evolution of the total reactant probability density, $P_{R,T}(t)$. The dashed line is the total reactant probability density and the solid line best biexponential fit to $P_{R,T}(t)$. The parameters from the fit lead to the values for the two rate constants of $\kappa^- = 2.2 \times 10^{-6}$ au for the tunneling rate and $\kappa^+ = 2.3 \times 10^{-4}$ au for the above the barrier rate. The thin line in Figure 5b shows the evolution of the below the barrier component of the wavepacket, that is, $P_R^-(t)$. The thicker solid line in Figure 4b shows the best fit of $P_R^-(t)$ to a single, decaying, exponential. We extract out a rate constant for tunneling from the exponential fit in Figure 5b and find, in this case, $\kappa^- = 2.6 \times 10^{-6}$ au. We extract out a rate constant for above the barrier product production from the exponential fit to $P_R^+(t)$ and find, in this case, $\kappa^+ = 2.2 \times 10^{-4}$ au.

All the results described thus far were for symmetric double-well potentials, that is, potentials that result from diabatic states with the same frequencies, $\omega_R = \omega_P$. Now we see if the quantum dynamics is separable into tunneling and above the barrier components for asymmetric potentials. In Figure 6, we show results for a double well potential with $\omega_R = 1500$ and 2000 cm^{-1} with nonadiabatic coupling strength of $g_0 = 150$ kJ mol^{-1}. In this case the barrier has a value of $E_A = 45$ kJ mol^{-1}. We consider the dynamics of an initial reactant wavepacket that is displaced by an amount $\delta x = 0.25$ Å at $t = 0$. With this displacement and this potential, the initial below and above the barrier probability densities are $P_R^-(t = 0) = 0.75$ and $P_R^+(t = 0) = 0.25$, respectively. In Figure 6a, we show the evolution of the total reactant probability density, $P_{R,T}(t)$. Again, the solid line is approximation to the total reactant probability density obtained when we separate it into it is $P_R^-(t)$ and $P_R^+(t)$components and the dashed line in Figure 6a is the exact total reactant probability density. Since the solid and dashed lines are in close agreement, the dynamics of the system is separable into below and above the barrier probability densities even for asymmetric double-well potentials. The solid line in Figure 6b shows the evolution of the below the barrier component of the wavepacket, that is, $P_R^-(t)$. The dashed line in Figure 6b shows the best fit of $P_R^-(t)$ to a single,

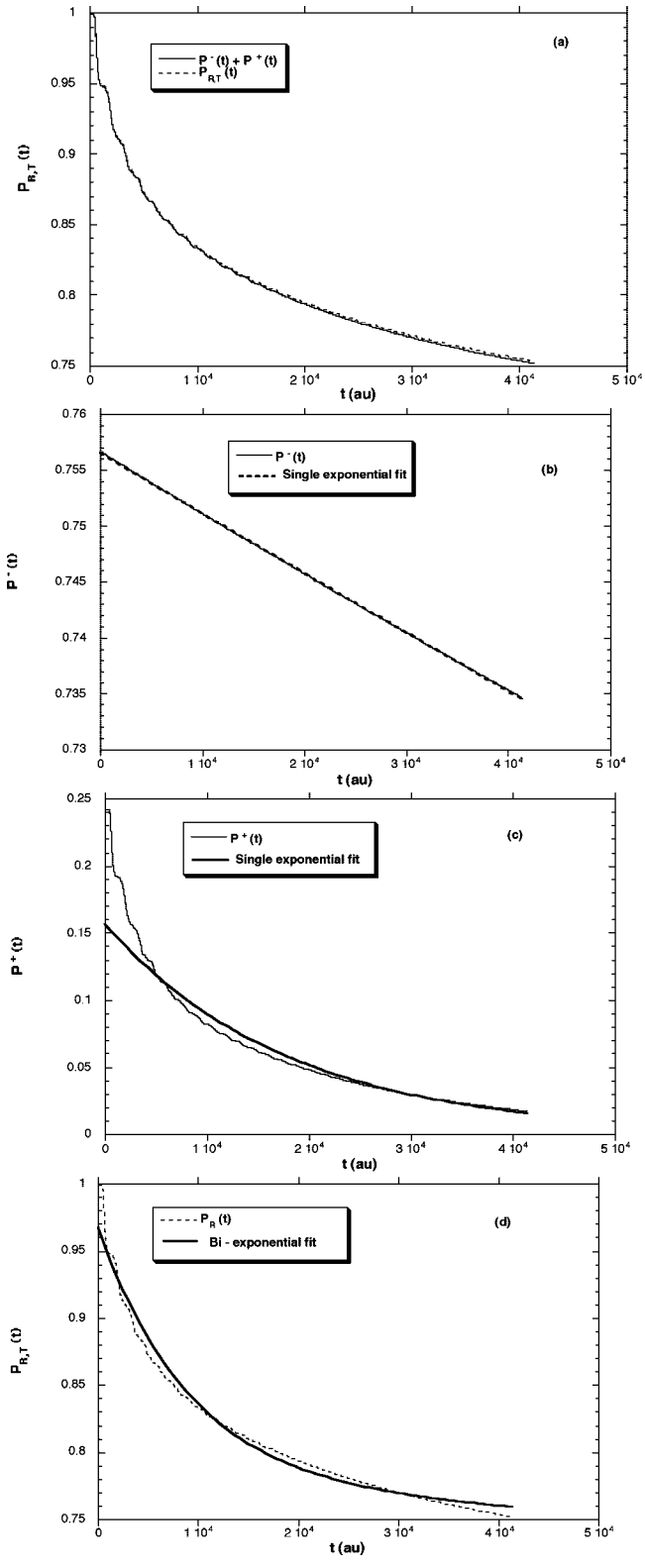

Figure 6. Evolution of the reactant probability density, $P_R(t)$ in the asymmetric double-well potential as discussed in the text and an initial displacement of $\delta x = 0.25$ Å: (a) the exact total reactant probability density (dashed line) and the approximate probability density (solid line). (b) The evolution of the below the barrier probability density, $P_R^-(t)$ (thin solid line) and the best single exponential fit (thick solid line). (c) Evolution of the above the barrier probability density, that is, $P_R^+(t)$ (thin solid line) and the best exponential fit (thick solid line). (d) The biexponential fit to the reactant probability density, $P_R(t)$, (solid line) and the exact total reactant probability density (dashed line).

decaying, exponential. Again, the tunneling dynamics is well represented by a single exponential. We extract out a rate constant for tunneling from the exponential fit in Figure 6b and find, in this case, $\kappa^- = 7 \times 10^{-7}$ au. This is an order of magnitude smaller than the tunneling rate constant for the symmetric potential with the same barrier, that is, $E_A = 45$ kJ mol^{-1} discussed in Figure 2. The thin line in Figure 6c shows the time evolution of the above the barrier probability density, $P_R^+(t)$. The thick solid line in Figure 6c shows the best single decaying exponential fit to $P_R^+(t)$. Again, the single exponential fit of $P_R^+(t)$ is not as good as that of $P_R^-(t)$ the fit does follow the overall decay trend pretty well. We extract out a rate constant for above the barrier product production from the exponential fit in Figure 6c and find, in this case, $\kappa^+ = 6.5 \times 10^{-5}$ au. In Figure 6d, we show the decay of the total reactant probability density in time with the dashed line. The solid line is the best biexponential fit to $P_{R,T}(t)$. The parameters from the fit lead to the values for the two rate constants of $\kappa^- = 6 \times 10^{-7}$ au for the tunneling rate and $\kappa^+ = 1 \times 10^{-4}$ au for the above the barrier rate. Again, these would be the rates that could be extracted from experimentally measured data. The rate constant for tunneling extracted in this way compares very well to the unobservable, but calculable, tunneling rate in Figure 6b of $\kappa^- = 7 \times 10^{-7}$ au.

Now we explore the isotope effect on the tunneling rate constant, κ^-. We study the same potential as in Figures 4. The potential parameters of $\omega_R = \omega_P = 2000$ cm^{-1} and a nonadiabatic coupling strength of $g_0 = 150$ kJ mol^{-1} leading to a barrier height of $E_A = 125$ kJ mol^{-1}.

Now we change the mass of the system to that of a D atom, $m = 2\ m_H$. When the system had the mass of the H atom there were 12 eigenstates below the barrier, now with the D atom there are 16 eigenstates below the barrier. This is consistent with the decrease in spacing between the energy levels with increasing mass. We study the quantum dynamics of the system when the initial wavepacket is displaced an amount $\delta x = 0.25$ Å at $t = 0$. In Figure 7a, we show the time evolution of the total reactant probability density, $P_{R,T}(t)$ with the dashed line and the best biexponential fit with the solid line. The fit parameters lead to values of $\kappa^- = 5.4 \times 10^{-7}$ au and $\kappa^+ = 9.6 \times 10^{-5}$ au. Note that the tunneling rate constant was $\kappa^- = 2.2 \times 10^{-6}$ au for the same potential and initial conditions for the H atom. As expected the rate constant is significantly smaller, by nearly an order of magnitude, for tunneling of the heavier D atom. In Figure 7b, we show the time evolution of the below the barrier component of the wavepacket, that is, $P_R^-(t)$. The thicker solid line in Figure 7b shows the best fit of $P_R^-(t)$ to a single, decaying, exponential. Again, the tunneling dynamics is well represented by a single exponential. We extract out a rate constant for tunneling from the exponential fit in Figure 6b and find, in this case, $\kappa^- = 5.4 \times 10^{-7}$ au. This rate constant closely agrees to the experimentally observable value obtained from the biexponential fit. Although, not shown, we fit the above the barrier probability density to a single exponential and found that it agrees with that of the biexponential fit, that is, $\kappa^+ = 9.6 \times 10^{-5}$, within 5%.

We now say a little more about the assumption that the two dynamic events, that is, tunneling and over the barrier

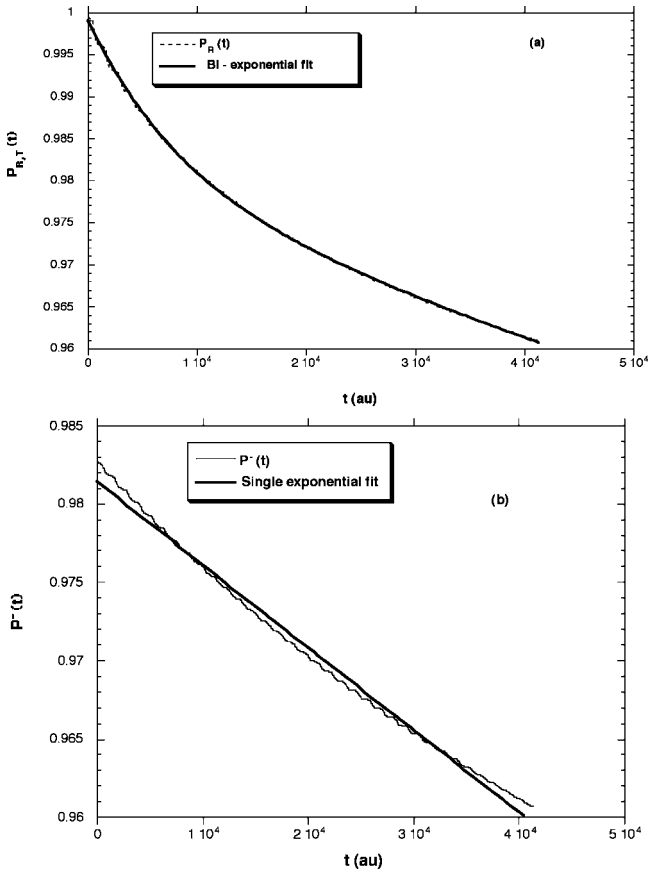

Figure 7. Evolution of the reactant probability density, $P_R(t)$ for deuterium in a double-well potential with a barrier height of 125 kJ mol^{-1} and an initial displacement of $\delta x = 0.25$ Å: (a) the exact total reactant probability density (dashed line) and the biexponential fit (solid line). (b) The evolution of the below the barrier probability density, $P_R^-(t)$ (thin solid line) and the best single exponential fit (thick solid line).

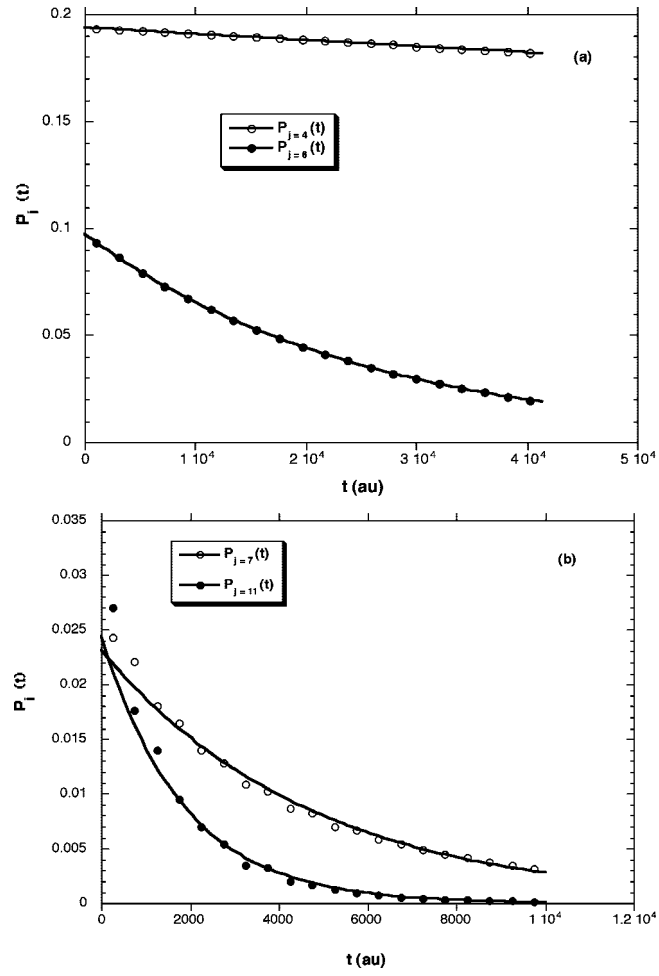

Figure 8. Evolution of the individual eigenstates as discussed in the text for a barrier of 45 kJ mol^{-1} and an initial displacement of $\delta x = 0.25$ Å: (a) the evolution of the $j = 4$ (open circles) and $j = 6$ (solid circles) below the barrier eigenstates. The solid lines are the best, single, exponential fits to each. (b) the evolution of the $j = 7$ (open circles) and $j = 11$ (solid circles) above the barrier eigenstates. The solid lines are the best, single, exponential fits to each.

production, can be treated as first order events. In Figure 8, we show the decay of some of the individual eigenstates for a barrier height of $E_A = 45$ kJ mol^{-1} and initial wavepacket displacement of $\delta x = 0.25$ Å. [The same system as that described by Figures 2.] As described previously, there are 6 eigenstates below the barrier and of these 6 only $j = 2, 4, 6$ contribute appreciably to the initial wavepacket superposition. In Figure 8a, we show the decay of the $j = 4$ and 6 eigenstates with the open and solid circles, respectively. The solid line shows a single, decaying, exponential fit to each. As shown by Figure 8a, each eigenstate decays exponentially and the aggregate decay of the below the barrier eigenstates, that is, the function $P_R^-(t)$, should be more accurately represented by the weighted sum of decaying exponentials as shown below.

$$P_R^-(t) = \sum_{j=1}^{m} |c_{j,0}|^2 \cdot e^{-\kappa_j t} \tag{35a}$$

In eq 35, the $\{c_{j,0}\}$are obtained from eq 20b, and the $\{\kappa_j\}$ are the decay constants for the eigenstates. In Figure 8a, the decay constants for the $j = 4$ and 6 eigenstates are $\kappa_4 = 1.6 \times 10^{-6}$ au and $\kappa_6 = 3.9 \times 10^{-5}$ au. Although not shown in Figure 8a, we have found the decay constant for the $j = 2$ eigenstate is $\kappa_2 = 1.8 \times 10^{-8}$ au. We define a weighted average of these below the barrier decay constants as

$$\langle \kappa^- \rangle = \sum_{j=1}^{m} |c_{j,0}|^2 \cdot \kappa_j \tag{36a}$$

This weighted average yields an average decay for the below the barrier eigenstates as $\langle \kappa^- \rangle = 5.5 \times 10^{-6}$ au. This compares favorably to the single exponential fit to $P_R^-(t)$, which had an exponent of $\kappa^- = 7.5 \times 10^{-6}$ au.

In Figure 8b, we show the decay of $j = 7$ and 11, both above the barrier eigenstates with the open and solid circles, respectively. The solid line shows a single, decaying, exponential fit to each. Again, both of the individual eigenstates decay exponentially. The $j = 7$ eigenstate is the first above the barrier eigenstate, and it decays with a decay constant of $\kappa_7 = 2.1 \times 10^{-4}$ au. This is a very revealing result. The energy separation between the last below the barrier eigenstate ($j = 6$) and the first above the barrier eigenstate ($j = 7$) is only 8 kJ mol$^{-1,}$ but the decay constant

of the above the barrier, $j = 7$, eigenstate is nearly 2 orders of magnitude larger. For comparison, the $j = 7$ and 8 eigenstates are also separated by about 8 kJ mol^{-1} in energy, but the decay constant for the $j = 8$ eigenstate is $\kappa_8 = 2.3 \times 10^{-4}$ au, that is, nearly the same as the $j = 7$ eigenstate. Further, the $j = 11$ eigenstate, shown via the solid circles in Figure 8b, has a decay constant of $\kappa_{11} = 5.4 \times 10^{-4}$ au, only twice as large as the $j = 7$ eigenstate, even though it is nearly 40 kJ mol^{-1} higher in energy. In fact, all the above the barrier eigenstates between $j = 7$ and $j = 15$, have decay constants that range between $\kappa = 2.1 \times 10^{-4}$ au and 8×10^{-4} au. In other words, the above the barrier eigenstates decay on almost identical time scales and the aggregate decay, that is, $P_R^+(t)$, are well quantified by a single decay constant that can be obtained from the weighted average

$$\langle \kappa^+ \rangle = \sum_{j=m+1} |c_{j,0}|^2 \cdot \kappa_j \tag{36b}$$

The results of the analysis accompanying Figures 8 verify the conjecture that there are really two dynamic events that can lead to H atom transfer, tunneling and above the barrier production, and these events are well separated in time. The results also explain how a comparison of the time scales of these two events can be well quantified by treating each as a single, first-order event. Each above the barrier eigenstate is well represented by a decaying exponential and all decay with nearly the same rate constant. Thus, the aggregate decay of the above the barrier components given by the function $P_R^+(t)$ can be considered to decay with an overall decay constant given by the weighted average in eq 36b. The below the barrier eigenstates, the ones responsible for tunneling, also, individually, decay exponentially although there is a wide disparity between the decay rates among the below the barrier eigenstates. More importantly, though, all of the below the barrier eigenstates decay much slower than even the least energetic above the barrier eigenstate. This demonstrates that the main conjecture of the present work is correct: There are two dynamic events that can accompany H atom transfer; they operate on different time scales, and it is possible to quantify the rates of each of these two events.

The results also show that one must be very careful when assigning a time scale, a rate constant, or a portion of a rate constant resulting from product production through tunneling. The results show that even though tunneling occurs on a much different time scale than above the barrier production of product, there is a wide disparity between the rates of tunneling between the individual, below the barrier, eigenstates. We suggest a way to ascribe a rate constant for tunneling is to consider the tunneling as an overall first-order process that represents reactant decay with a rate constant, κ^-, given by the weighted average in eq 36a, although other definitions are possible.

IV. Conclusion

In this work we described a rationale for defining and determining a "tunneling rate" from experimental observables of an H atom transfer reaction. The key to this view is the energetic decomposition of an initial H atom wavepacket into above and below the barrier components. This wavepacket decomposition was defined in such a way as to satisfy two criteria. The first criterion is that these two wavepacket components must evolve independently of one another in time. The second criterion is that a time-evolving probability density can be assigned, separately, to each component. We have shown that both of these criteria can be satisfied if the two wavepacket components are formed by superpositions of the eigenstates of the potential energy under which they evolve.

We stress here that the major conclusion of this work is *not* that one can calculate a tunneling rate constant from a simulation using the wavepacket decomposition as described above. The major conclusion of this work is that such a simple, and perhaps obvious way to decompose an initial reactant wavepacket, leads to a rational way for an experimentalist to interpret observables in a kinetics experiment on an H atom transfer reaction. We have shown that a biexponential fit to the overall decay of reactant (the observable) can be used to extract out a rate constant for tunneling alone. The simulations merely serve to show that the less negative of the two exponents in the bi-exponential fit is the one that describes the tunneling rate, and the more negative describes over the barrier product production. We have shown that two, pre-exponential terms in the fit give information about the initial, nonequilibrium, state of the system. Again, the simulations merely serve to show that the pre-exponential term in front of the less negative exponential can be interpreted as the percent of the initial wavepacket that has energy less than the barrier and the other pre-exponential term gives the percent of the initial wavepacket above the barrier. As the pre-exponential term in front of the less negative exponential decreases, there is less of the initial H atom wavepacket below the barrier, and this can be interpreted as meaning that the system is prepared in a state farther from equilibrium at $t = 0$. Thus, an experimentalist can gain from a single experimental observable, the overall decay of reactant concentration, kinetic, *and* structural information about the H atom transfer reaction.

We have also found that, via simulations, that the energetic decomposition of the initial reactant wavepacket leads to a bi-exponential decay of reactant concentration for symmetric and asymmetric potentials and for differing isotopes of the H atom.

Another conclusion from this work is that a short-time exponential fit of reactant concentration decay has very little to do with the rate of tunneling. The initial decay of reactant concentration is dominated by the faster dynamic event, over the barrier product production.

Finally, we discuss how the coupling between the H atom reaction coordinate, x, and other degrees of freedom can effect the present results and conclusions. We will also sketch out a way toward treating such multidimensional systems.

We classify two types of coupling to the H atom reaction coordinate: (1) direct coupling and (2) bilinear coupling to vibrational modes. By direct coupling, we mean that the single-dimensional potential energy, $V^*(x)$, would be replaced by a multidimensional potential of the form, $V^*(x,\vec{y})$, where $\{\vec{y}\}$are some small set of other degrees of freedom that directly effect the evolution of the H atom wavepacket. For

example, if each of the diabatic surfaces $V_P(x)$ and $V_R(x)$ were two-dimensional, that is,

$$V_R(x,y) = \frac{m\omega_R^2}{2}[(x-y) - (x_R^0 - y_R^0)]^2 \qquad (37)$$

the resulting double-well adiabatic potential would be a nontrivially coupled two-dimensional potential. One could envision that such direct coupling between the H atom coordinate, x, and the y degree of freedom would have a large effect on both tunneling and above the barrier product production. In fact, the effect might be large enough to make the time scales of the two dynamic events become too close to distinguish. This, by no means, should detract from the relevance of the present work. In fact, results of the present work would indicate that if there were *not* an observable separation of time scales in the H atom transfer event, then other effects such as the strong coupling mentioned above could be present.

The other type of coupling that could be present is bilinear coupling of the H atom transfer coordinate to a set of vibrational modes, $\{\vec{\eta}\}$. In this case the double-well potential, $V^*(x)$, would be replaced by a potential energy of the form,

$$V^*(x,\vec{\eta}) = V^*(x) + \frac{1}{2}\sum_{k=1}\omega_k^2 \cdot (\eta_k - c_k \cdot x)^2 \qquad (38)$$

where ω_k and c_k are frequencies and coupling of the kth mode to the H atom coordinate, respectively. The major effect of such coupling would be to serve as a sink of energy for the H atom coordinate. If the coupling were strong enough then it might be possible for the above the barrier eigenstates to have decay constants approaching those of the below the barrier eigenstates. Thus, in the strong coupling case, the time scales of tunneling and above the barrier transfer could become too close to distinguish. Again, this should not detract from the relevance of the present work because the absence of two distinguishable time scales in the transfer event would indicate such strong coupling was present.

We now describe how one could generalize the present work to treat the two types of multidimensional systems described above. If the H atom reaction coordinate, x, was directly coupled to one or two degrees, of freedom, $\vec{y}$, then the generalization of the present work would be straightforward. For example, if the H atom reaction coordinate were coupled to a single degree of freedom, one would calculate the eigenenergies, $\{E_n\}$, and eigenfunctions, $\{\psi\}$, of the two-dimensional potential, $V^*(x,y)$. There would now be many more eigenstates above and below the barrier, but as in the present work, we would not have to propagate each one separately in time, just propagate two groupings: $\Psi^-(x,y,t)$ the group of below the barrier eigenstates and $\Psi^+(x,y,t)$ the group of above the barrier eigenstates. The propagation of each could be accomplished by solving the TDSE on a two-dimensional spatial grid instead of the single-dimensional grid used in the single-dimensional case.

If the H atom reaction coordinate, x, was bilinearly coupled to a set of vibrational modes, $\{\vec{\eta}\}$, the procedure described above could not be used. The reason is that, presently, there is an upper limit of 4−5 degrees of freedom for solving the TDSE on a spatial grid. The simplest and least accurate way to treat this type of multidimensional system would be to treat the oscillators classically. In this case, the above the below and above the barrier eigenstates, $\Psi^-(x,t)$ and $\Psi^+(x,t)$, would still be single dimensional, but they would be propagated via time-dependent potential, $V^*(x,\vec{\eta}_t;t)$, that depended parametrically on the instantaneous positions, $\{\eta_t\}$, of each vibrational mode. The trajectory of each vibrational mode would be determined via the Verlet algorithm, where each vibrational mode experienced a force, $F_j = -\sum_{k=1}\omega_k^2 \cdot (\eta_k - c_k \cdot \langle x\rangle_t)$, that depended on the expectation value, $\langle x\rangle_t$, of the H atom position.

Acknowledgment. Financial support of this work was provided by the Henry Dreyfus Teacher-Scholar Awards Program.

References

(1) Klinman, J. P.; Liang, Z-X. *Curr. Opin. Struct. Biol.* **2004**, *14*, 648.

(2) Borman, S. *Chem. Eng. News.* **2004**, *82*, 35.

(3) Warshel, A.; Papazyan, A. *Proc. Natl. Acad. Sci. U.S.A.* **1996**, *93*, 13665.

(4) Gertlt, J. A.; Kreevoy, M. M.; Cleland, W. W.; Frey, P. A. *Chem. Biol.* **1997**, *4*, 259.

(5) Bruice, C. T. *Acc. Chem. Res.* **2002**, *35*, 1.

(6) Klinman, J. P. *Pure Appl. Chem.* **2003**, *75*, 601.

(7) Mincer, J. S.; Schwartz, S. D. *J. Phys. Chem. B* **2003**, *107*, 366.

(8) Benkovik, S. J.; Hammes-Schiffer, S. *Science* **2003**, *301*, 1198.

(9) Hammes-Schiffer, S. *Biochemistry* **2002**, *41*, 13335.

(10) Antoniou, D.; Schwartz, S. D. *J. Chem. Phys. B* **2001**, *105*, 5553.

(11) Poulsen, T. D.; Garcia-Viloca, M.; Gao, J.; Truhlar, D. G. *J. Phys. Chem. B* **2003**, *107*, 9567.

(12) Alhambra, C.; Corchado, J.; Sanchez, M. L.; Garcia-Viloca, M.; Gao, J.; Truhlar, D. G. *J. Phys. Chem. B* **2001**, *105*, 11326.

(13) Warshel, A.; Chu, Z. T. *J. Chem. Phys.* **1990**, *93*, 4003.

(14) Hammes-Schiffer, S.; Tully, J. C. *J. Phys. Chem.* **1995**, *99*, 5793.

(15) Mincer, J. S.; Schwartz, S. D. *J. Phys. Chem. B* **2003**, *107*, 366.

(16) Hur, S.; Bruice, T. C. *J. Am. Chem. Soc.* **2003**, *125*, 10540.

(17) Hur, S.; Bruice, T. C. *Proc. Natl. Acad. Sci. U.S.A.* **2003**, *100*, 12015.

(18) Reddy, S. Y.; Bruice, T. C. *J. Am. Chem. Soc.* **2003**, *126*, 2431.

(19) Kramers, H. A. *Physica* **1940**, *7*, 284.

(20) Hanggi, P.; Talkner, P.; Borkovec, M. *Rev. Mod. Phys.* **1990**, *62*, 251.

(21) Feit, M. D.; Fleck, J. A.; Steiger, A. *J. Comput. Phys.* **1982**, *47*, 412.

(22) Marquardt, D. W. *J. Soc. Ind. Appl. Math.* **1963**, *11*, 431.

CT800436U